Forecasting Equatorial Spread F and the Prereversal Enhancement using WAM-IPE

Aaron Kirchman[1], David Hysell[1], Tzu-Wei Fang[2], Tim Fuller-Rowell[2,3]

[1]Cornell University, Ithaca, NY

[2]Space Weather Prediction Center, Boulder, CO

[3]University of Colorado, Boulder, CO

Introduction & Objectives:

Equatorial Spread F (ESF) is the name given to a collection of plasma irregularities commonly observed in the equatorial F region ionosphere near sunset. These irregularities can cause scintillation of radio signals that traverse the region. An example of coherent scatter radar observations of an ESF event is shown in Fig. 1.

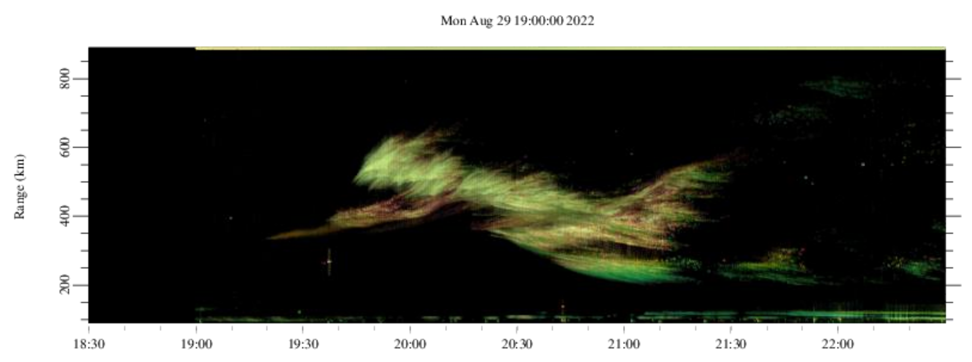

Fig. 1: Range-Time-Intensity (RTI) of coherent scatter radar data during a strong ESF event on 29 Aug. 2022. Hue, saturation, and brightness of each pixel represent SNR, Doppler velocity, and spectral width, respectively

A regional physics-based simulation is used to reproduce irregularities associated with ESF, as an initial forecast of ESF. First, the simulation is initialized and driven with ISR observations. Next, WAM-IPE electric fields are substituted in to drive the simulation. **Results indicate that inaccuracies in the day-to-day variation of WAM-IPE vertical drifts fail to generate accurate day-to-day estimates of ESF activity.** A proxy electrodynamics model is developed to test two sensitivities: neutral winds and enhanced molecular ion densities.

Regional Simulation:

The regional simulation is described in detail in Hysell et al. (2014). There are two primary components: a 3-dimensional potential solver that enforces a divergence-free current density, and a finite-volume code that advances number densities of 4 ion species (H^+, He^+, NO^+, O^+) and electrons in time.

$$\nabla\cdot(\sigma\cdot\nabla\Phi) = \nabla\cdot\left[\sigma\cdot(\mathbf{E}_0+\mathbf{u}\times\mathbf{B}) + \sum_s q_s \mathbf{D}_s\cdot\nabla n_s + \Xi\cdot\mathbf{g}\right] \qquad \frac{\partial n_s}{\partial t} + \nabla\cdot(n_s\mathbf{v}_s) = P_s - L_s$$

The simulation is initialized and driven with ISR observations alongside various empirical and physics-based models (SAMI2, NRLMSIS 2.0, IRI-2016, HWM14). Blank patches in ISR data (shown below) act as an indicator of ESF activity.

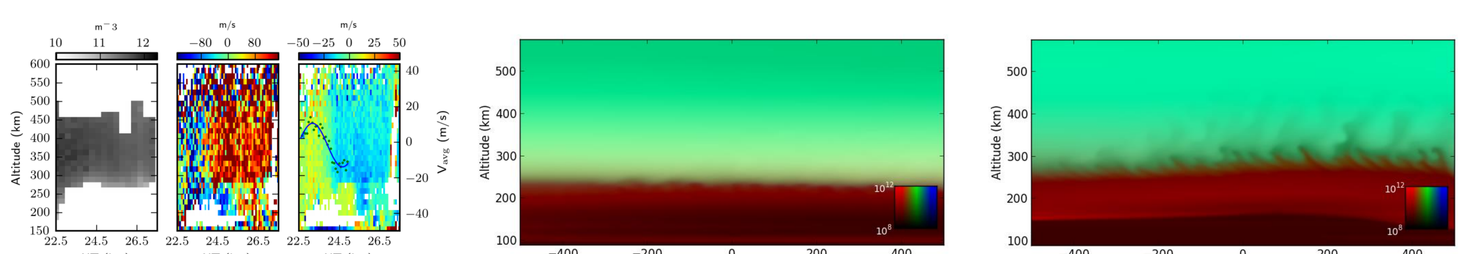
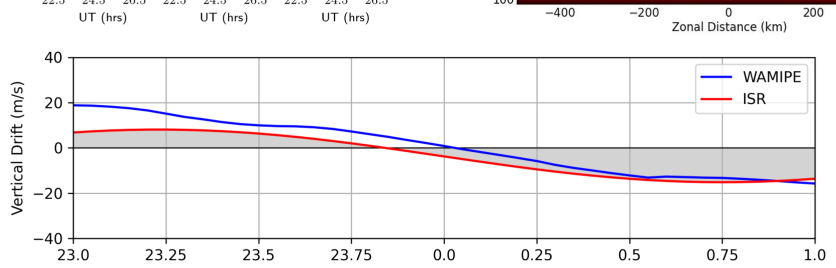

Fig. 2: Simulation results for 25/26 Sept. 2021, when no ESF was observed. Top: (left) ISR data showing no strong ESF irregularities, (center) simulated density 2 hours after initialization when driven with ISR data, (right) simulated density when driven with WAMIPE E-fields. Bottom: Vertical plasma drifts from ISR and WAMIPE. Red, green, and blue coloring indicates molecular, hydrogen, and atomic oxygen ions, respectively.

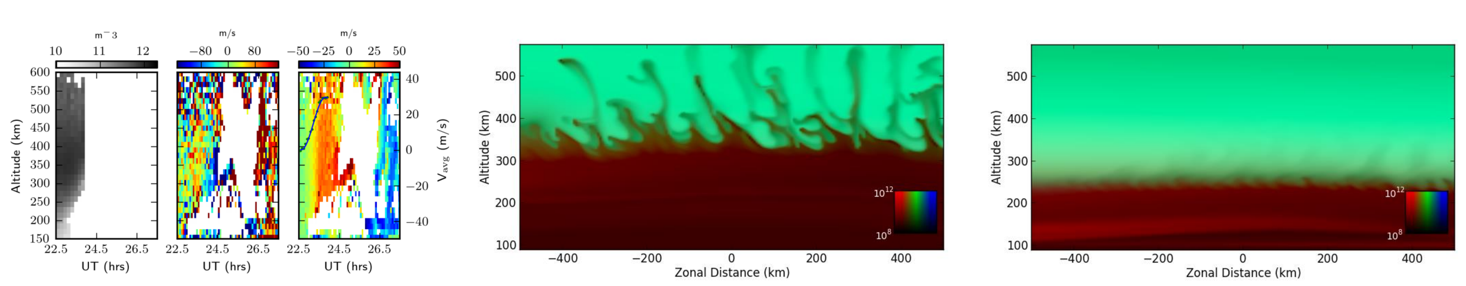
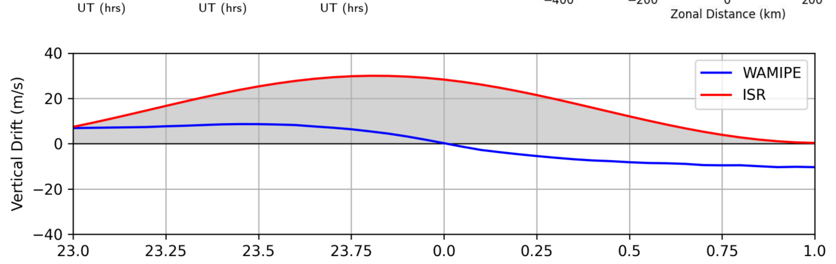

Fig. 3: Same as Fig. 2, but for 29/30 Aug. 2022, when strong ESF activity was detected and reproduced using ISR data, but not when using WAMIPE background E-fields.

Note the **strong disagreement in vertical plasma drifts between ISR observations and WAM-IPE values.** This disagreement is most prevalent on nights when WAM-IPE electric field driven simulations failed to reproduce observed ESF activity. Additionally, there is a connection between large vertical drifts and a late reversal time with the presence of ESF. This observation agrees with Fejer et al. (1999). This all emphasizes the importance of accurate vertical drifts in an ESF forecast.

Fig. 4: ISR observed vertical plasma drifts for all nights during 2021 and 2022 campaigns. Green (red) lines indicate nights where ESF was observed (was not observed). Note the connection between large upward drifts and late reversal times with ESF events.

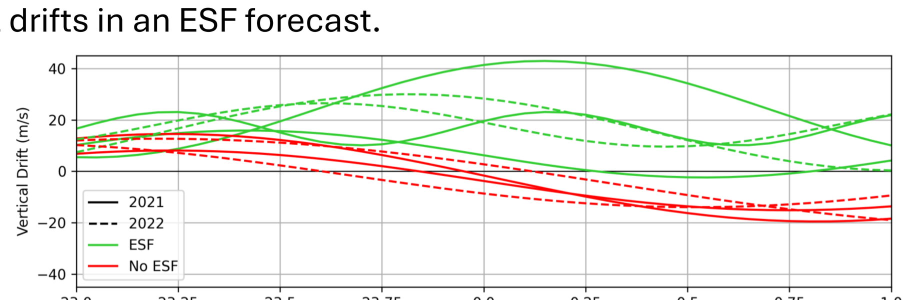

Proxy Electrodynamics Model:

To consider the impacts of different driving factors for the WAM-IPE background electric fields, a simplified proxy model for WAM-IPE electrodynamics is developed. This proxy model is a two-dimensional, field-line integrated model cast in dipole coordinates, (q, p, φ), for field-line tracing, and circular polar coordinates, (L, ϕ), in the magnetic equatorial plane. The model is similar to that described by Haerendel et al. (1992).

$$\frac{\partial}{\partial L}\left[L\Sigma_P\frac{\partial\Phi}{\partial L}\right] + \frac{\partial}{\partial\phi}\left[\frac{\tilde{\Sigma}_P}{L}\frac{\partial\Phi}{\partial\phi}\right] + \frac{\partial\Sigma_H}{\partial\phi}\frac{\partial\Phi}{\partial L} - \frac{\partial\Sigma_H}{\partial L}\frac{\partial\Phi}{\partial\phi} = R_E\left(\frac{\partial[LS_L]}{\partial L} - \frac{\partial S_\phi}{\partial\phi}\right)$$

$$\Sigma_P = \frac{1}{L}\int\sigma_P\frac{h_q h_\varphi}{h_p}dq \qquad S_L = \frac{1}{LR_E}\int B\left(\sigma_P u_\varphi + \sigma_H u_p\right)h_q h_\varphi dq$$

$$\tilde{\Sigma}_P = L\int\sigma_P\frac{h_q h_p}{h_\varphi}dq \qquad S_\phi = \frac{1}{R_E}\int B\left(\sigma_P u_p - \sigma_H u_\varphi\right)h_q h_p dq$$

$$\Sigma_H = \int\sigma_H h_q dq$$

First, **the model is solved using WAM-IPE parameters** to reproduce WAM-IPE electric fields. Next, **HWM14 winds are used to replace the neutral winds from WAM-IPE**. Finally, based on simulation results in Fig. 2-3, the **molecular ion density is decreased to 10% of their values in WAM-IPE**. The resulting changes to integrated values are shown in Fig. 5, and their effects on the vertical plasma drifts are shown in Fig. 6-7.

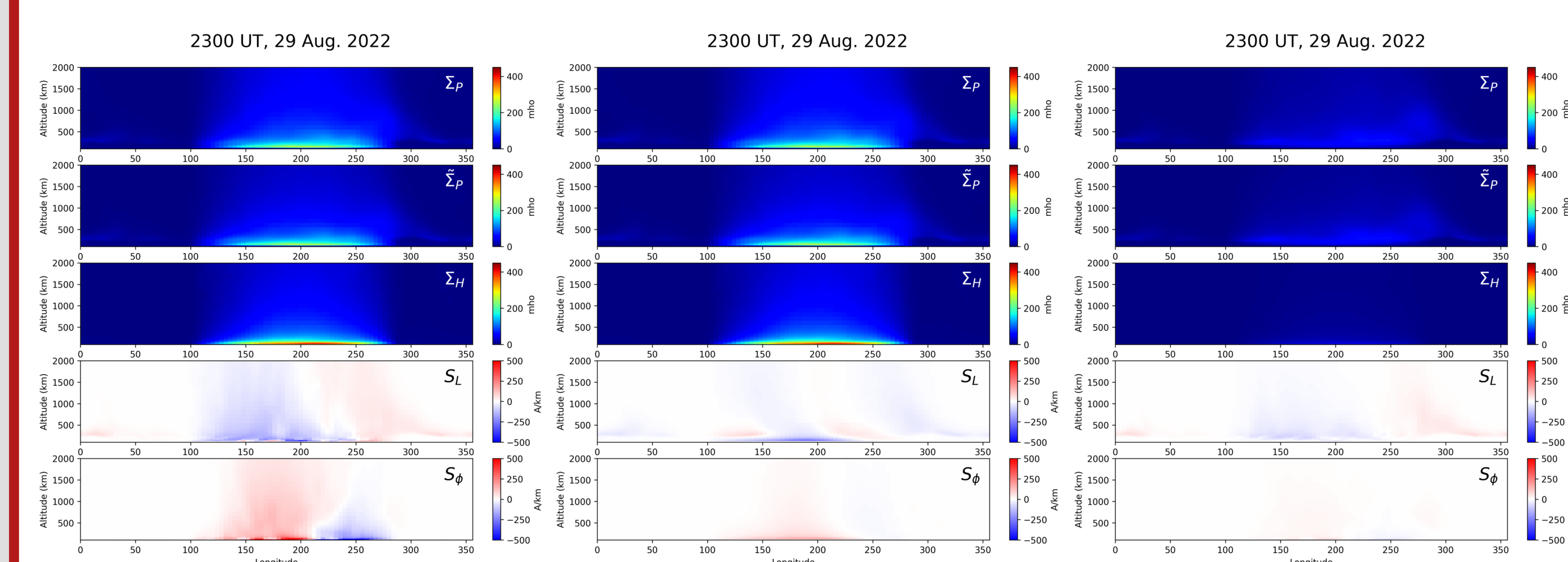

Fig. 5: Integrated values used in the proxy electrodynamics solver. The definitions of these are given to the left. Left: WAM-IPE parameters. Center: WAM-IPE Composition, HWM14 Winds. Right: Decreased WAM-IPE molecular ion density, WAM-IPE Winds.

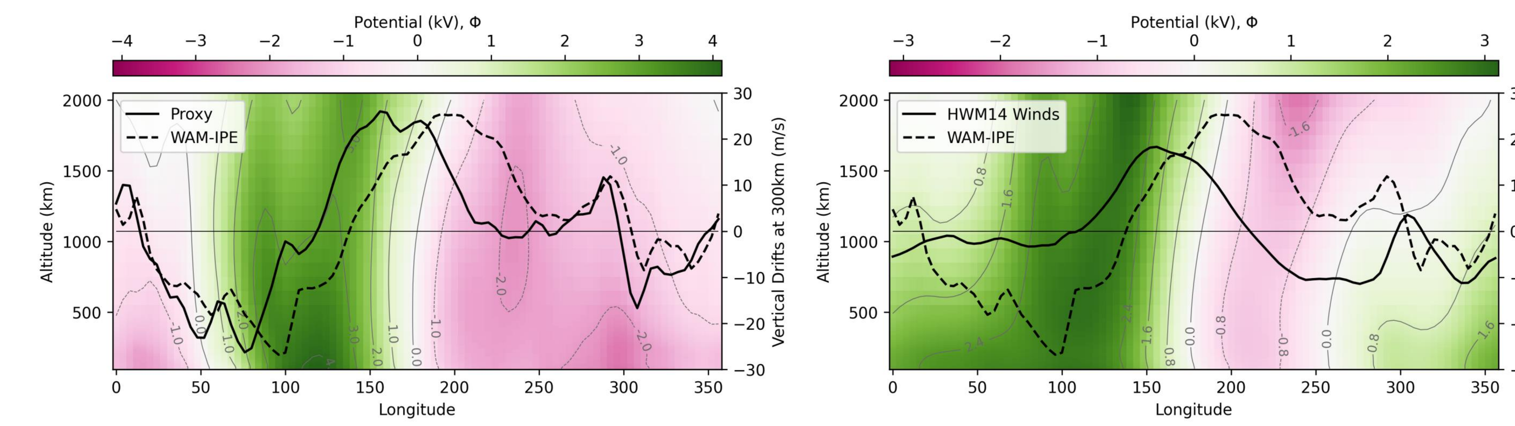
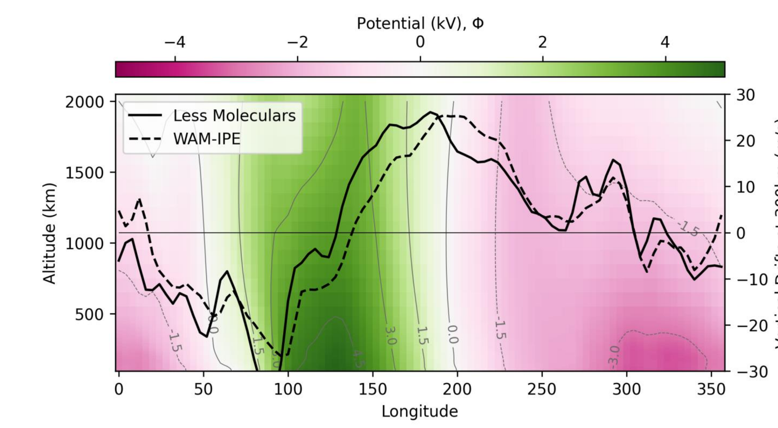

Fig. 6: Electrostatic potential solutions to the proxy model. The resulting vertical drifts (solid line) and the WAM-IPE vertical drifts (dashed line) are plotted against the right axis in each panel. Top Left: WAM-IPE parameters. Top Right: WAM-IPE Composition, HWM14 Winds. Bottom Left: Decreased WAM-IPE molecular ion density, WAM-IPE Winds.

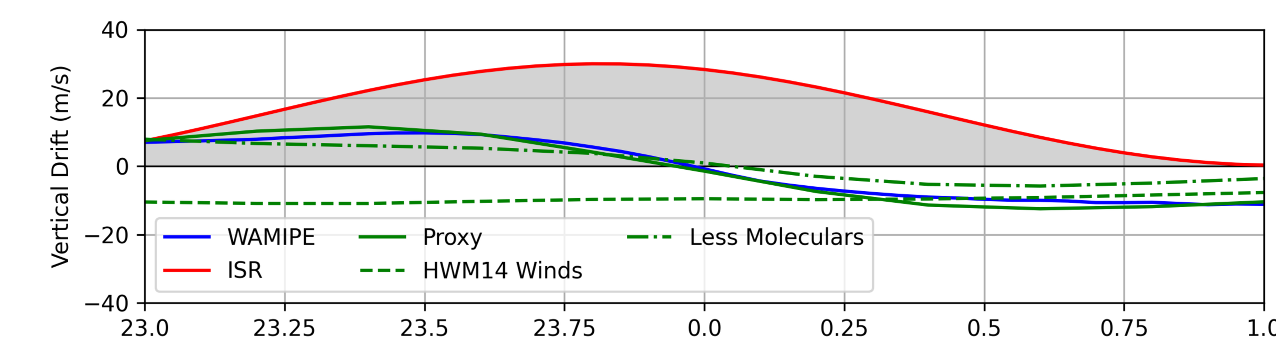

Fig. 7: Vertical plasma drifts overhead Jicamarca. ISR measurements, WAM-IPE values, and proxy model solutions are shown.

The proxy model is able to recreate time series of vertical drifts from WAM-IPE. **Neither substitution in this study resulted in drifts that were more comparable to ISR observations.** More tests are needed to understand how exactly the composition and neutral winds cause the development of the PRE.

Persistency of PRE in WAM-IPE:

The timing, magnitude, and duration of the PRE has a strong effect on the generation of ESF activity (Fejer et al. (1999), and others). This enhancement of the zonal electric fields follows a structure like that shown in Fig. 8. **At any two times in UT, the two enhancements shown in Fig. 8 are expected to fall nearly on top of one another.** This is not necessary the case for WAM-IPE vertical plasma drifts.

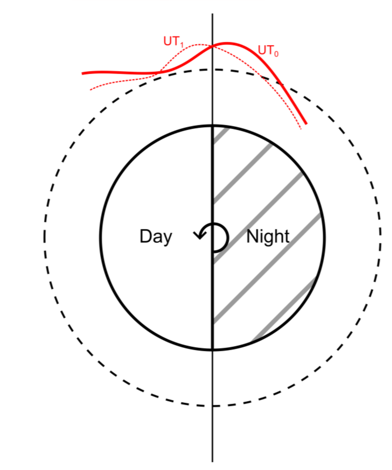

Fig. 8: Sketch of the typical location and shape of the evening prereversal enhancement from WAM-IPE at two different UTs.

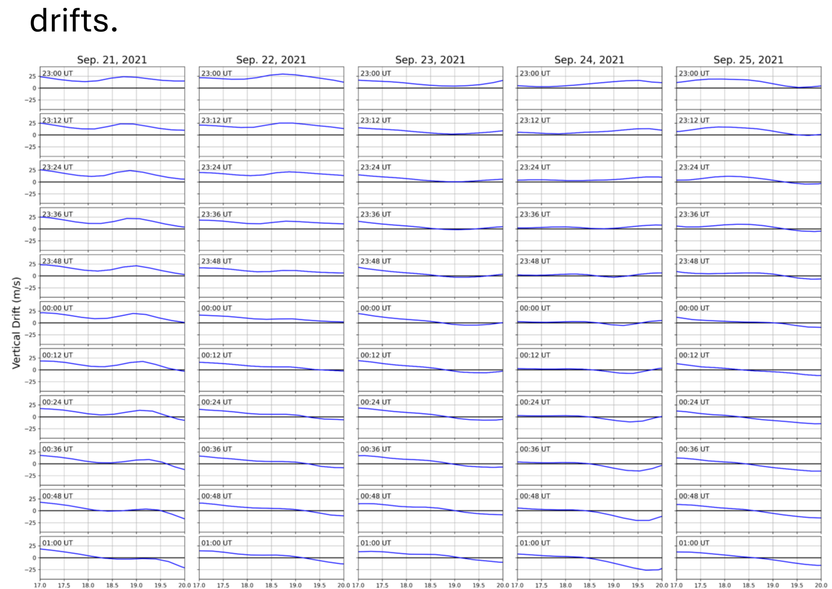

Fig. 9: Vertical plasma drifts taken from WAM-IPE at varying UT times surrounding the terminator in LT (longitude) for the 2021 campaign.

Taking the correlation function between the vertical plasma drifts at two UTs emphasizes the **rapid variation of the PRE present in WAM-IPE.** Fig. 10 shows the variation in the persistence of the structure of the PRE. In particular, nights similar to 30 Aug. 2022 represents the expected persistence. Nights similar to 24 Sept. 2021 exhibit poor persistence.

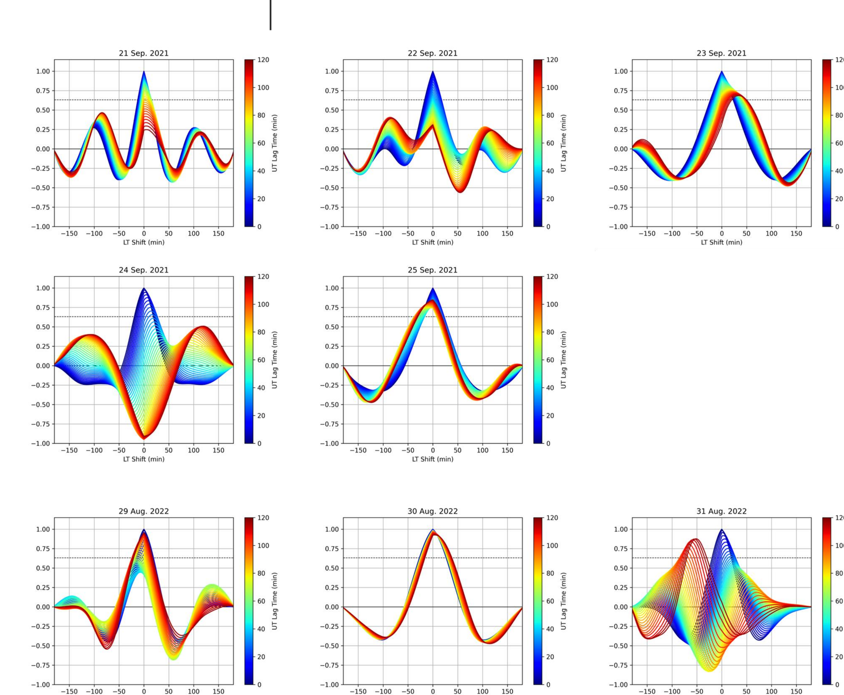
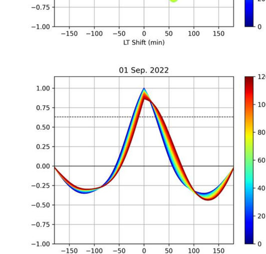

Fig. 10: Correlation functions of the vertical plasma drifts taken from WAM-IPE. The horizontal axis is LT (longitudinal) shift relative to the day/night terminator. The color of the functions represents the lag time in UT between samples being correlated. Top: 2021 campaign. Bottom: 2022 campaign.

Conclusions:

Results from a regional simulation of ESF activity driven by WAM-IPE highlight the **importance of accurate vertical plasma drift measurements for an ESF forecast.** The inaccurate day-to-day variation in WAM-IPE vertical drifts was studied with the proxy electrodynamics model. **Neither a direct substitution of HWM14 neutral winds, nor a decrease in molecular ion density produced vertical drift time series comparable to ISR observations.** Future studies with the proxy model are necessary to generate vertical drifts that can be used in a forecast. Additionally, future studies are needed to understand the persistency of, or lack thereof, the PRE structure.

Future Work:

- Further analysis of WAM-IPE vertical plasma drifts and their ability to accurately drive the regional simulation.
- Provide more sensitivity tests for the proxy electrodynamics, which may provide direction for future studies of WAM-IPE background electric fields.
- Determine the persistency of the PRE structure in nature through ICON satellite measurements
  - Preliminary results (Hysell et al. (2024)) suggests the PRE is well-correlated in shape and position across at least 104 min.
- Generate a new regional model using extended MHD theory that will run in real-time, or near real-time, providing a more reasonable forecast and prediction of ESF activity.

References:

Fejer, B. G., Scherliess, L., & de Paula, E. R. (1999). Effects of the vertical plasma drift velocity on the generation and evolution of equatorial spread F. *Journal of Geophysical Research: Space Physics*, *104*(A9), 19859–19869. https://doi.org/10.1029/1999JA900271

Haerendel, G., Eccles, J. V., & Çakir, S. (1992). Theory for modeling the equatorial evening ionosphere and the origin of the shear in the horizontal plasma flow. *Journal of Geophysical Research: Space Physics*, *97*(A2), 1209–1223. https://doi.org/10.1029/91JA02226

Hysell, D. L., Fang, T. W., & Fuller-Rowell, T. J. (2022). Modeling Equatorial F-Region Ionospheric Instability Using a Regional Ionospheric Irregularity Model and WAM-IPE. *Journal of Geophysical Research: Space Physics*, *127*(9), e2022JA030513. https://doi.org/10.1029/2022JA030513

Hysell, D. L., Jafari, R., Milla, M. A., & Meriwether, J. W. (2014). Data-driven numerical simulations of equatorial spread F in the Peruvian sector. *Journal of Geophysical Research: Space Physics*, *119*(5), 3815–3827. https://doi.org/10.1002/2014JA019889

Hysell, D. L., Kirchman, A., Harding, B. J., Heelis, R. A., England, S. L., Frey, H. U., & Mende, S. B. (2024). Using ICON Satellite Data to Forecast Equatorial Ionospheric Instability Throughout 2022. *Space Weather*, *22*(3), e2023SW003817. https://doi.org/10.1029/2023SW003817